Mixing rates and symmetry breaking in two-dimensional chaotic flow

Greg A. Voth,[a] T. C. Saint, Greg Dobler, and J. P. Gollub[b]
Department of Physics, Haverford College, Haverford, Pennsylvania 19041

(Received 11 February 2003; accepted 4 June 2003; published 31 July 2003)

We experimentally determine the mixing rate for a magnetically forced two-dimensional time-periodic flow exhibiting chaotic mixing. The mixing rate, defined as the rate of decay of the root-mean square concentration inhomogeneity, grows with Reynolds number, but does not increase at the onset of nonperiodic (weakly turbulent) flow. The mixing rate increases linearly with a second non-dimensional parameter, the typical path length of a fluid element in one forcing period. The breaking of time-reversal symmetry and spatial reflection symmetry substantially increases the mixing rates. A theory by Antonsen *et al.* that predicts mixing rates in terms of the measured Lyapunov exponents of the flow is tested and found to predict mixing rates that are too large by approximately a factor of 10; the discrepancy is traced to the fact that large scale transport rather than stretching of fluid elements is the dominant rate limiting step when the system is sufficiently large compared to the velocity correlation length. An effective diffusion model gives a good account of the measured mixing rates. Finally, the formation of persistent recurrent patterns (also called strange eigenmodes) is shown to arise from a combination of stretching and effective diffusion.
 [DOI: 10.1063/1.1596915]

I. INTRODUCTION

A central goal of the study of fluid mixing is to understand and predict the rate at which an initially inhomogeneous fluid is homogenized. Extensive studies of mixing have yielded many insights into the geometric structures that govern the mixing process, particularly in two-dimensional (2-D) flows.[1–3] This picture has benefited greatly from the application of the theory of dynamical systems to mixing, starting with Aref,[4] but these insights have not been easily extended to understanding mixing rates.

A variety of conceptual frameworks have been developed for understanding and predicting mixing rates. Melnikov-type methods work well for understanding mixing rates when the flow is nearly integrable,[5] but many flows of interest are not in this limit.[1] Approaches based on the stretching produced by the flow include ''mixing efficiency''[1] and calculations based on the finite time Lyapunov exponents.[6,7] Recently, it has been recognized that persistent spatial patterns, also called strange eigenmodes,[8,9] must be considered in the prediction of mixing rates.[10,11] Consideration of symmetries of the flow can provide important insights into the rate of fluid mixing. Certain symmetries in the flow field guarantee that the flow is integrable, which in turn implies very slow mixing.[12–14]

In this paper, we present experimental measurements of mixing rates in a two-dimensional flow that produces chaotic mixing. In this well-characterized magnetically forced flow,[15,16] it is possible to measure simultaneously the dye concentration fields, velocity fields, and stretching fields.[17] Using these measurements, we explore the essential elements that must be incorporated in a theory to explain the mixing rates.

The primary results of this paper include the following: (1) Several symmetries of the flow are identified and their importance as impediments to mixing are evaluated. (2) Two effects that might be expected to affect mixing rates, the transition to non-periodic flow, and geometric resonances in transport, do not have a measurable affect. (3) Mixing rates are more accurately predicted by an effective diffusion model than by a model based on finite time Lyapunov exponents. This leads to the conclusion that attempts to predict mixing rates in large systems must include transport as well as stretching rates. (4) Understanding transport mechanisms in this flow allows deeper insight into the processes that create periodic persistent patterns.[16]

II. EXPERIMENT

We study mixing in an electromagnetically driven fluid layer as shown in Fig. 1. A sinusoidal electric current travels horizontally through a fluid layer that is placed above an array of permanent magnets. The resulting Lorentz forces drive a vortex array flow in the fluid. The magnets are configured either randomly or on a regular grid as shown in Fig. 1. In order to have a 2-D layer with negligible shear across it, a less dense non-conducting fluid layer 1 mm thick floats on the conducting layer. The fluids are mixtures of glycerin and water; the lower layer contains NaCl (3 M concentration) to make it conductive. The two layers remain distinct for the duration of an experiment, roughly 20 min, even though they are miscible.

For most of the experiments reported in this paper, half of the upper layer is initially marked with sodium fluorescein dye (concentration 7.5×10^{-5} M) and the other half is un-

[a]Currently at Department of Physics, Wesleyan University, Middletown, CT 06459.
[b]Also at Department of Physics, University of Pennsylvania, Philadelphia, PA 19104. Electronic mail: jgollub@haverford.edu

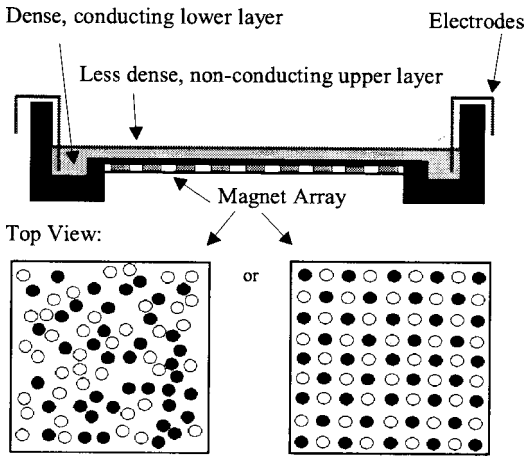

FIG. 1. Diagram of the two-dimensional, magnetically forced, time-periodic flow.

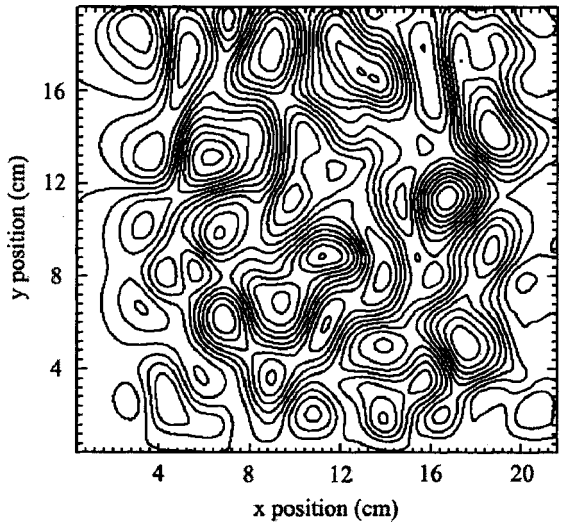

FIG. 2. Instantaneous stream function of the flow driven by the random magnet configuration at Re=100 and $p=5$. The flow is instantaneously a random vortex array whose form is distorted with time, but that repeats periodically.

dyed. The diffusivity of fluorescein is $D=5\times10^{-10}\,\mathrm{m^2\,s^{-1}}$. A small quantity of Photoflo is used to decrease the effects of surface tension. The driving current is controlled by placing the cell in the feedback loop of an operational amplifier circuit, which ensures that the current follows a specified waveform, even though the effective resistance varies with time as a result of ion accumulation near the electrodes. We use ac forcing with frequencies in the range 20–200 mHz. The use of ac forcing ensures that any net fluid motion over a full period is a consequence of nonreversibility of the flow. During one period T of the flow, diffusion spreads dye over a length $L=\sqrt{2DT}$, which sets the smallest length scales of the dye pattern in the range of 0.2–0.07 mm.

The fluid is illuminated in the near UV, and images of the dye patterns are acquired with a Sensicam cooled CCD camera from the Cooke Corp. This system provides 12 bit monochrome images at 1280×1024 resolution, with readout rate up to 8 frames/s to computer memory. A glass plate covering the cell is necessary to eliminate ambient air currents, so that the fluid's velocity field is not measurably influenced by environmental variations.

The stream function of the flow when driven by the random magnet array is shown in Fig. 2, at an instant when the rms velocity is near its maximum. The stream function is calculated from separate experiments in which velocity fields are measured by video particle tracking. For these experiments, the flow is seeded with fluorescent polystyrene spheres of diameter 120 μm, which float at the interface between the two fluid layers. Video imaging and particle tracking software allow the extraction of individual particle trajectories. Because the flow is periodic, we can average velocity measurements at the same phase and obtain very high spatial resolution. Details about the particle tracking measurements are available in an earlier paper.[17]

There has been significant discussion in the literature of the degree to which this flow models an ideal 2-D system. There is good evidence that the velocity field is two dimensional when the forcing time scale is long compared with the vertical momentum transport time. We estimate the vertical momentum transport time to be less than 1 s based on the results in Ref. 15, and our forcing period is always longer than 5 s, so we are confident that the velocity field is nearly 2-D.

A separate question however is the degree to which the flow is a solution to the 2-D Navier–Stokes equation. It clearly cannot be, unless a term in addition to the body forcing term is included to account for the viscous stresses in the vertical direction. Since the vertical profile is approximately of Poiseuille form,[15] a term proportional to the velocity may be sufficient. This effect would have to be considered if the experiments presented here were compared to 2-D Navier–Stokes simulations. We do not undertake such a comparison here.

There are two important non-dimensional parameters for this flow. The Reynolds number $\mathrm{Re}=UL/\nu$ is based on the mean magnet spacing $L=2$ cm, rms velocity U, and kinematic viscosity ν. The second parameter is the path length $p=U/Lf$ traveled by a typical fluid element in one forcing period $1/f$, normalized by L. The Strouhal number $\mathrm{St}=p^{-1}$ could be used instead, but we prefer p because of its simple physical interpretation.

Both Re and p are experimentally controlled by adjusting the forcing current, its frequency, and the fluid viscosity. We wish to compare mixing rates while one of the nondimensional parameters is held constant, so we require the ability to choose particular Re and p. Since the relationship between the experimental control parameters and the rms velocity cannot easily be calculated analytically, we have instead measured the empirical relationship using particle tracking.

A convenient parametrization of the measured rms velocities is provided by modeling the flow as a sinusoidally driven damped mass:

$$\ddot{x}=-\omega_0\dot{x}+F_0\sin(\omega t), \tag{1}$$

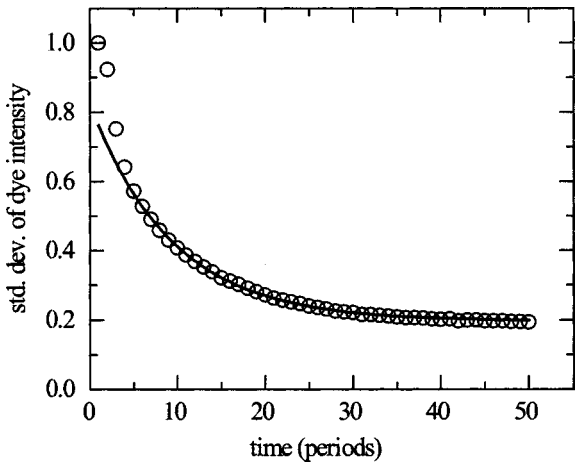

FIG. 3. Standard deviation of the dye intensity as a function of time for $p=5$, Re=100. The solid line shows a fit of Eq. (3) to the time range from 6 to 35 periods.

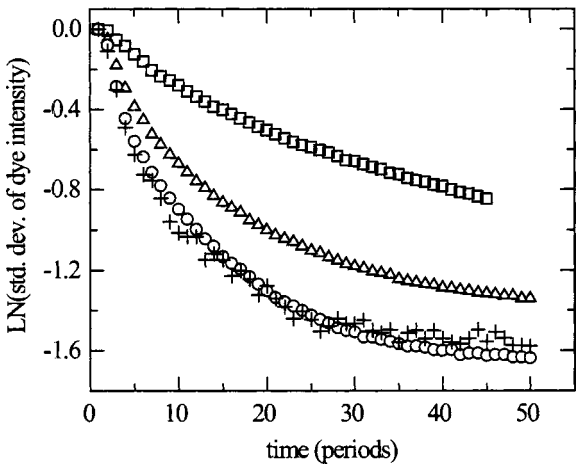

FIG. 4. Standard deviation of dye intensity as a function of time for $p=5$. (□) Re=25; (△) Re=55; (○) Re=100; (+) Re=170. The decay rate of the variance grows with Re and saturates beyond Re≈100.

where x is the position of the mass, ω_0 and F_0 are independent of time, and $\omega=2\pi f$ is the driving frequency. This model accurately reproduces the reduced response and phase delay that grow as ω is increased. We expect that the dependence on the driving current can be taken into account by allowing for a linear variation of F_0 with the current, so we write $F_0=\Gamma I$. Solutions for the velocity are of the form

$$\dot{x}=\frac{\Gamma I}{\sqrt{1+(\omega/\omega_0)^2}}\sin(\omega t+\delta). \tag{2}$$

We identify $\dot{x}$ with the rms velocity in the flow. By measuring the rms velocity over a range of currents and frequencies, we determine the constants Γ and ω_0 for each solution with different viscosity that is used. Equation (2) then provides a parametrization that predicts the velocity and hence the Reynolds number and path length for any current and frequency. We find that this approach allows us to obtain any desired combination of dimensionless parameters Re and p, with accuracy of better than 10%, by adjusting the forcing current, its frequency, and the fluid viscosity.

III. RESULTS

A. Measurement of mixing rates

Full characterization of the process of homogenization of an impurity in a flowing fluid requires recording the space and time dependence of the impurity concentration field. However, for many purposes it is advantageous to have a single number to characterize the mixing rate. To this end, we first identify the spatial standard deviation of the instantaneous impurity concentration field as a measure of the degree of mixing that has occurred. Figure 3 shows this quantity as a function of time during a typical mixing run. Also shown is a fit of the function

$$\langle C^2\rangle^{1/2}=C_0\exp(-Rt)+C_1 \tag{3}$$

to the concentration decay curve, where C_0, R, and C_1 are fit parameters. Throughout this paper we refer to the quantity R determined by this fitting procedure as the measured mixing rate.

This functional form is a convenient parametrization, not a rigorous model. Clearly, the inclusion of the constant C_1 reflects non-ideal factors since the concentration standard deviation would be expected to decay to zero in the long time limit. Experimentally we find that there are measurable concentration fluctuations even when premixed fluid is used for the upper layer. This is caused by weak three-dimensional flows which decrease the thickness of the upper layer in some regions, for example in the centers of vortices. In addition, we find that the value of R has a measurable dependence on the time interval used in the fit, typically decreasing as the time interval is moved to larger t. We interpret this as resulting from the slow process of transport of fluid initially trapped near the no slip boundaries. The measurement errors we report for R are dominated by this variation between fits to different parts of the decay curve.

Figure 4 shows the time dependence of the concentration variance for a series of runs at different Reynolds number but constant $p=5$. A fit to each of these provides the measured mixing rates which are plotted in Fig. 5. Qualitatively, the mixing rate data appear very much as expected. R increases monotonically upon increase of the Reynolds number. A plot of the mixing rate at different p but constant Re is shown in Fig. 6. Here the two different curves are for the two different magnet configurations, both at Re=80. Again, qualitatively, the data are not surprising. The mixing rate increases with path length. However, careful consideration of the mixing rate data reveals several significant insights which are described in the following sections.

B. Effects of symmetry breaking on mixing rates

A striking feature in the mixing rates is that the flow undergoes a transition to temporally nonperiodic flow, but there is no signature of this transition in the mixing rates. This transition occurs via a kind of period-doubling bifurca-

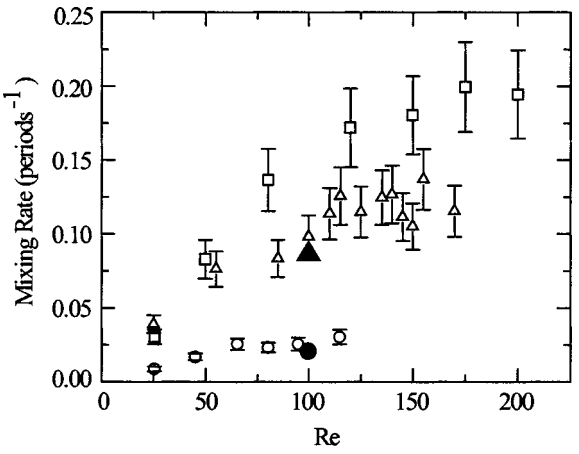

FIG. 5. Measured mixing rates (R) as a function of Reynolds number. (□) $p=8$; (△) $p=5$; (○) $p=2$. The mixing rate grows with Re and with path length p. The two closed symbols are the predictions of the decay rates from an effective diffusion process. (▲) $p=5$ and Re=100; (●) $p=2$ and Re =100.

tion. This can be observed in Fig. 7, which shows images taken once per period of three flows at $p=5$ but with different Re. For Re=85, the flow is periodic and the images show a persistent pattern. Careful observation of the images from Re=115 shows that the pattern repeats every other period: the flow has period-doubled. For Re=170, the flow no longer shows any time periodicity. We have also observed period-four behavior at $p=5$, Re=125, which is not shown. The onset of turbulence is identified with the development of space–time disorder,[18] of which an important element is the appearance of temporal non-periodicity. Since turbulence is often identified with effective mixing, it is interesting to check whether the onset of temporal non-periodicity leads to faster mixing. Surprisingly, we find that in the experiments reported here, the onset of non-periodicity does not lead to a change in either the mixing rate, or in the rate of growth of the mixing rate with Re. Therefore, non-periodicity alone is not the primary feature that enables turbulent flows to mix effectively. Rather than the breaking of time periodicity, it is

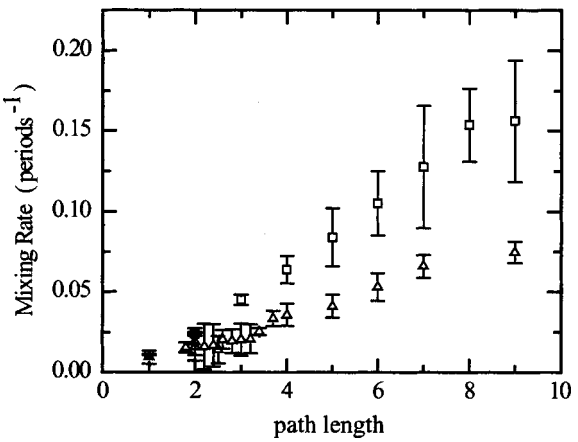

FIG. 6. Measured mixing rate (R) as a function of path length at Re=80. (□) Random magnet configuration; (△) regular magnet configuration. The mixing rate grows with path length and is reduced for the regular configuration by barriers to transport.

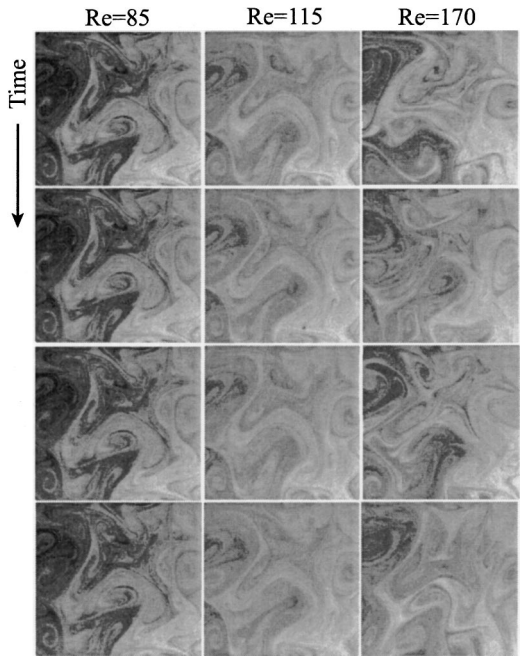

FIG. 7. Images of the dye field showing the transition to non-periodic flow. Each column shows a different Reynolds number. Each row shows an image taken one period after the row above it. At Re=85, the flow is periodic and the pattern repeats once per period. At Re=115, the dye field repeats only once every other period, i.e., it has period doubled. At Re=170 the dye field is non-periodic, or weakly turbulent.

the breaking of time reversal and spatial symmetries that turn out to be the dominant symmetry-related features affecting mixing.

Another way to show the transition to non-periodic flow is to plot the deviation from periodicity of the velocity field, which is shown in Fig. 8(a). The difference in the velocity at two times separated by one period should be zero when the flow is periodic. By calculating the standard deviation of this quantity, averaged over space and time, we obtain a measure of the breaking of time periodicity. Particle tracking is used for these measurements, although the data sets are relatively small in order to allow many Reynolds numbers to be studied. The results show a clear loss of time-periodicity above Re=150. There is significant scatter, partly due to the fact that these experiments combine many different path lengths. No signature of period-doubling is visible in these data, probably because the deviations in the period-doubled velocity fields are quite small.

While the flow loses *time periodicity* at a definite Reynolds number, the presence of chaotic mixing implies that it must have a breaking of *time reversal symmetry* even at very small Reynolds numbers. Otherwise, each particle would return exactly to its starting point once per period, and there could be no chaotic mixing. Figure 8(b) shows a measure of the breaking of time-reversal symmetry. The sum of the local velocities at equal time intervals before and after the zero crossing of the velocity should be zero if there were time reversal symmetry. The standard deviation of this quantity, again averaged over space and phase, is plotted in Fig. 8(b). (One detail is that the zero of velocity does not occur at exactly the same instant at all spatial locations, so we use as

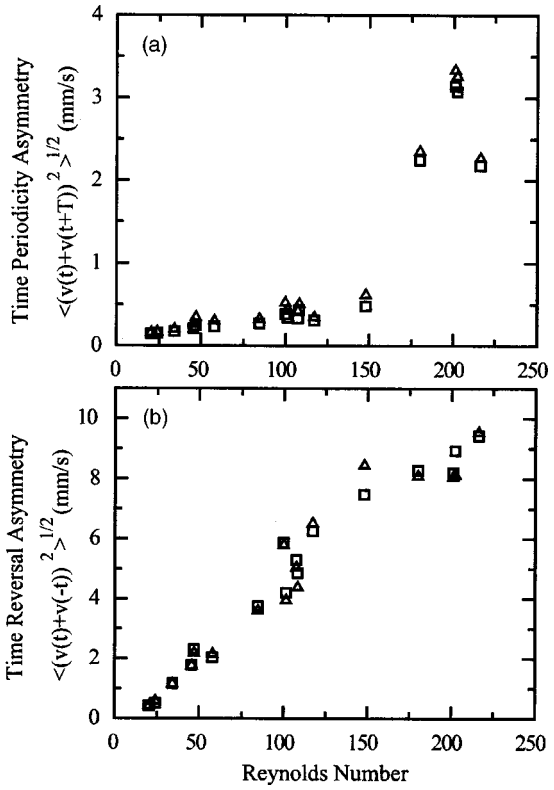

FIG. 8. (a) Degree of non-periodicity in the velocity field. The standard deviation of the difference between the velocity fields at two times separated by one period is shown as a function of Reynolds number. (□) The velocity component along the current direction, (△) the perpendicular velocity component. (b) Degree of non-time-reversibility of the velocity field, defined as the standard deviation of the difference between the velocity fields at equal intervals before and after the instant of smallest velocity. Symbols are the same as in (a). Note that the flow loses its time reversal symmetry long before it becomes non-periodic.

our reference instant the time of minimum velocity magnitude, averaged across the entire flow.) The degree of time reversal symmetry breaking grows smoothly with Re starting at very small Re.

Symmetry considerations also explain the fact that the regular magnet configuration is found to mix more slowly than the random array (Fig. 6). This can be attributed to the barriers to mixing created by the spatial symmetry of the regular array. This flow has many lines across which the flow has approximate reflection symmetry. If this symmetry were perfect, the fluid velocity perpendicular to these lines would be required to be zero, and hence these lines act as barriers to transport. Small deviations from perfect symmetry (e.g., due to variations in magnet placement or strength) allow some fluid to be transported across these lines; however, the barriers still significantly reduce the mixing rate.

Numerical[19] and experimental[20] studies of wavy Taylor–Couette flow have found that axial transport rates, and hence mixing rates, first increase and then decrease with increasing Reynolds number. Mezic[5] provides a theoretical explanation of this phenomenon, implying that the decrease may be a universal feature of chaotic flows. This explanation relies on the fact that with increasing Reynolds number, the flow approaches an inviscid (Euler) flow. Except for special cases like the ABC flow, inviscid flows are integrable; and so the mixing rate at high Reynolds number should go to zero. Our data (Fig. 5) do not show this predicted decrease with Reynolds number, although the slope does decrease. It remains possible that a decreasing mixing rate with increasing Reynolds number would exist if the transition to non-time-periodic flow did not occur first.

A further prominent feature in the mixing rate data is the smooth linear relation in Fig. 6 between the homogenization rate and p. Computations by Solomon *et al.*[21] of a spatially periodic flow similar to that produced by the regular magnet array have found geometric resonances which enhance particle transport at certain path lengths. If geometrical resonances made a significant contribution to mixing in our flow, we would expect maxima in the mixing rates at specific values of p. There is no sign of such resonances in our data, although it is possible that their effects are smaller than the measurement errors. An important difference between our flow and the one studied by Solomon *et al.*[21] is that the barriers of reflection symmetry in their flow are broken by coherent oscillations of the vortex centers. In our flow, these barriers are broken by irregularities in the magnet configuration. Since transport across the lines of mirror symmetry is determined here by small deviations from perfect symmetry, mixing across the barriers between different pairs of cells can be very different. As a result global resonances in particle transport may be suppressed.

C. Predicting mixing rates

Our ability to measure both the decay of the dye concentration field and the statistics of the stretching field in the same flow allows us to compare the measured mixing rates with theoretical predictions based on the finite time Lyapunov exponents of the flow. Antonsen *et al.*[6] predict that the long time decay of the scalar concentration variance will obey

$$\langle c(t)^2\rangle \propto \int_0^\infty h^{1/2} dh\, P(h,t)\exp(-ht), \tag{4}$$

where $P(h,t)$ is the probability density of the finite time Lyapunov exponents (h) over time interval t. While this theory has been criticized for failing to adequately capture global mixing mechanisms,[10] it remains one of the only available explicit predictions of mixing rates.

When Eq. (4) is used with the measured probability density for finite time Lyapunov exponents,[17] the decay of concentration is found to be approximately exponential in time. However, we find that the predicted decay rate is nearly a factor of 10 larger than the measured mixing rate. There is significant uncertainty in this calculation because the prediction depends sensitively on the form of $P(h,t)$ near $h=0$, and experimentally the region near $h=0$ shows dependence on how we treat the boundaries. However, known effects cannot account for the factor of 10 discrepancy.

Comparison of the flow used in Ref. 6 with the present experiment reveals a major difference. They use a sine flow with periodic boundary conditions, whereas our flow has a spatial extent much larger than the velocity correlation

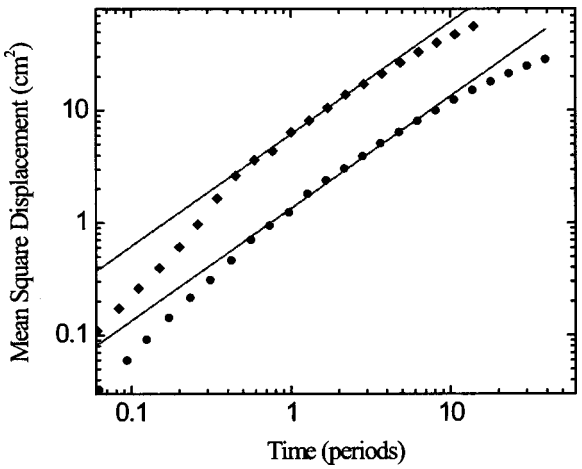

FIG. 9. Mean square displacement of particles for Re=100, $p=5$ (♦) and Re=100, $p=2$ (●). The solid lines show the linear (diffusive) scaling that best matches time range between 1 and 5 periods. These fits, along with Eq. (5), yield $\Gamma_{\text{eff}}=3.1$ cm^2/period and 0.67 cm^2/period, respectively.

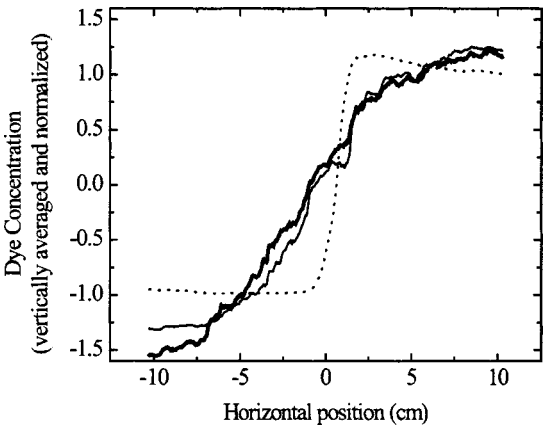

FIG. 10. Horizontal profile of the dye concentration at three different times. Images of the dye concentration, similar to those in Fig. 8, are vertically averaged; then the mean is substracted and the profile is normalized by its standard deviation. The normalized profile approaches the sinusoidal form of the slowest decaying diffusive mode. ($t=0$, dotted line; $t=6$ periods, solid line; $t=36$ periods, bold line. Random magnet configuration, $p=3$, Re=80.)

length. This difference in scale suggests that transport of impurity across the experimental flow may limit the measured mixing rate, whereas the theory assumes that the mixing rate is locally controlled by the stretching process.

To quantify the importance of transport across the flow, consider a model of mixing based on an effective diffusivity. The long time transport of fluid elements is primarily diffusive,[21,22] so the mean square displacement of particles can be used to define an effective diffusivity

$$\langle(\Delta x)^2\rangle = 2\Gamma_{\text{eff}}\, t. \tag{5}$$

The dye concentration decay rate in this model is then found by solving the diffusion equation in a closed box given the initial dye distribution. The problem is one dimensional, and is easily solved with a Fourier decomposition. The long time decay is dominated by the mode with the longest wavelength. Its decay rate is

$$R=\Gamma_{\text{eff}}\,(\pi/L)^2, \tag{6}$$

where L is the length of the flow in the direction of the concentration gradient.

Experimental measurements of the mean square displacement of particles are shown in Fig. 9. The time span over which the motion is diffusive is limited because the velocity correlation length (roughly, the magnet spacing) is only about one-tenth of the system size. However, it is still possible to determine an effective diffusivity that best fits the data.

Expected scalar decay rates that are determined from these effective diffusivities and Eq. (6) are plotted with closed symbols in Fig. 5. The agreement with the measured mixing rates is quite good for both data points. Further support of this effective diffusion picture is provided by Fig. 10, which shows the horizontal profile of the dye concentration field. When normalized to remove the contrast decay, the profile is found to approach the sinusoidal form of the slowest decaying mode in a diffusive process.

D. Persistent patterns

The recognition that transport through an effective diffusion process dominates the experimental mixing rate allows a new perspective on the development of persistent patterns in spatially extended chaotic flows. Consider two limiting systems. In the first, the length scale of the dye concentration field is large compared to the velocity correlation length. Our experimental system tends toward this limit, and here the rate limiting step in mixing is transport of fluid between independent regions of the flow. In the second limiting system, the spatial scale of the dye concentration field is much smaller than the velocity correlation length. In this case, the mixing rate is determined by the rate of stretching and folding of fluid elements, and the mixing rate may possibly be calculated using the approach of Antonsen *et al.*[6] However, Sukhatme and Pierrehumbert[11] have recently analyzed the importance of the relative length scales of the scalar and velocity field and concluded that even in this limit, the calculation based only on Lyapunov exponents may be incomplete for describing the long time scalar decay.

The processes that control the mixing rate in these two limiting cases are fundamentally distinct, but they have a remarkable feature in common. They both produce persistent patterns, i.e., the concentration field can be written as a function of space multiplied by an exponentially decaying function of time. In the diffusive case the spatial function is simply a sinusoid. In the stretching dominated case, the spatial function has been called a "strange eigenmode;"[8] its gradients are aligned with regions of large stretching which mark the unstable manifold of the flow.[3,23]

The experimental flow that we study lies between these two limiting cases. The persistent pattern that develops can thus be conceptually decomposed into small scale and large scale structures. The small scale structures contain the sharpest dye gradients, which are aligned by the stretching field. Since the stretching field is time-periodic, images taken once per period show that these small scale structures approach a

persistent pattern, defined by the lines that have experienced large stretching, which correspond to the unstable manifolds in the flow.[17] The large scale structure of the dye concentration field, on the other hand, is governed by transport, and is approximately a problem of effective (or eddy) diffusion. This large scale structure approaches its persistent pattern over a time that is somewhat longer than that required for the small scale pattern to develop. As a result, and because sharp gradients dominate visual perception, the pattern appears to approach a stationary pattern rather quickly. However, the averaged horizontal profile approaches a persistent pattern at a slower rate determined by transport across the system. The variance of the dye distribution can only decay as fast as transport allows the large scale structures to be removed, so this longer characteristic time dominates the mixing rate. In the experiment, these two processes do not have a large enough separation of scales to be fully distinguished; however, considering the limiting cases confirms that both of these fundamentally different processes are working together to produce the persistent patterns.

IV. CONCLUSIONS

In this paper, we have reported careful measurements of the rate at which an inhomogeneous scalar field becomes homogeneous in a two-dimensional flow exhibiting chaotic mixing. Specific space and time symmetries of the flow have been identified that provide a framework for understanding the mixing rates, especially the progressive breaking of time-reversal symmetry. We have discussed the results in terms of available theory, and have demonstrated the need to incorporate both stretching and transport in future theoretical models of homogenization. A simple ''effective diffusion'' model captures the mixing rates well in our flow, while stretching based models work well in smaller flows. A comprehensive approach is still needed to unite these two limiting cases.

ACKNOWLEDGMENTS

This work was supported by NSF Grant No. DMR-0072203. We appreciate helpful discussions with T. Antonsen, B. Eckhardt, I. Mezic, E. Ott, and J. L. Thiffeault. Laurent Montagnon made important contributions to the early stages of this experiment.

[1] J. M. Ottino, *The Kinematics of Mixing, Stretching, and Chaos* (Cambridge University Press, Cambridge, 1989).
[2] J. M. Ottino, ''Mixing, chaotic advection, and turbulence,'' Annu. Rev. Fluid Mech. **22**, 207 (1990).
[3] V. Rom-Kedar, A. Leonard, and S. Wiggins, ''An analytical study of transport, mixing and chaos in an unsteady vortical flow,'' J. Fluid Mech. **214**, 347 (1990).
[4] H. Aref, ''Stirring by chaotic advection,'' J. Fluid Mech. **143**, 1 (1984).
[5] I. Mezic, ''Chaotic advection in bounded Navier–Stokes flows,'' J. Fluid Mech. **431**, 347 (2001).
[6] T. M. Antonsen, Z. Fan, E. Ott, and E. Garcia-Lopez, ''The role of chaotic orbits in the determination of power spectra of passive scalars,'' Phys. Fluids **8**, 3094 (1996).
[7] A. K. Pattanayak, ''Characterizing the metastable balance between chaos and diffusion,'' Physica D **148**, 1 (2001).
[8] R. T. Pierrehumbert, ''Tracer microstructure in the large eddy dominated regime,'' Chaos, Solitons Fractals **4**, 1091 (1994).
[9] R. T. Pierrehumbert, ''Lattice models of advection-diffusion,'' Chaos **10**, 61 (2000).
[10] D. R. Fereday, P. H. Haynes, A. Wonhas, and J. C. Vassilicos, ''Scalar variance decay in chaotic advection and Batchelor-regime turbulence,'' Phys. Rev. E **65**, 035301 (2002).
[11] J. Sukhatme and R. T. Pierrehumbert, ''Decay of passive scalars under the action of single scale smooth velocity fields in bounded two-dimensional domains,'' Phys. Rev. E **66**, 056302 (2002).
[12] I. Mezic and S. Wiggins, ''On the integrability and perturbation of three dimensional fluid flows with symmetry,'' J. Nonlinear Sci. **4**, 157 (1994).
[13] G. Haller and I. Mezic, ''Reduction of three-dimensional volume-preserving flows with symmetry,'' Nonlinearity **11**, 319 (1998).
[14] G. King, G. Rowlands, M. Rudman, and A. Yannacopoulos, ''Predicting chaotic dispersion with Eulerian symmetry measures: Wavy Taylor-vortex flow,'' Phys. Fluids **13**, 2522 (2001).
[15] J. Paret, D. Marteau, O. Paireau, and P. Tabeling, ''Are flows electromagnetically forced in thin stratified layers two dimensional?'' Phys. Fluids **9**, 3102 (1997).
[16] D. Rothstein, E. Henry, and J. P. Gollub, ''Persistent patterns in transient chaotic mixing,'' Nature (London) **401**, 770 (1999).
[17] G. Voth, G. Haller, and J. P. Gollub, ''Experimental measurements of stretching fields in fluid mixing,'' Phys. Rev. Lett. **88**, 254501 (2002).
[18] P. Manneville, *Dissipative Structures and Weak Turbulence* (Academic, Boston, 1990).
[19] M. Rudman, ''Mixing and particle dispersion in the wavy vortex regime of Taylor–Couette flow,'' AIChE J. **44**, 1015 (1997).
[20] S. Wereley and R. Lueptow, ''Spatio-temporal character of non-wavy and wavy Taylor–Couette flow,'' J. Fluid Mech. **364**, 59 (1998).
[21] T. Solomon, A. Lee, and M. Fogleman, ''Resonant flights and transient superdiffusion in a time-periodic, two-dimensional flow,'' Physica D **157**, 40 (2001).
[22] G. I. Taylor, ''Diffusion by continuous movements,'' Proc. London Math. Soc. **20**, 196 (1921).
[23] F. Muzzio, P. Swanson, and J. Ottino, ''The statistics of stretching and stirring in chaotic flows,'' Phys. Fluids A **3**, 822 (1991).